Petroleum Science 20 (2023) 1598–1607

Contents lists available at ScienceDirect

Petroleum Science

journal homepage: www.keaipublishing.com/en/journals/petroleum-science

Original Paper

A novel nanofluid of modified carbon black nanoparticles for enhanced oil recovery in low permeability reservoirs

Guang Zhao [a, *], Li-Hao Liang [b], Dong-Fang Lv [a], Wen-Juan Ji [a], Qing You [c], Cai-Li Dai [a]

[a] School of Petroleum Engineering, China University of Petroleum (East China), Qingdao, 266580, Shandong, the People's Republic of China
[b] Research Institute of Petroleum Exploration & Development, PetroChina, Beijing, 100083, the People's Republic of China
[c] School of Energy Resources, China University of Geosciences (Beijing), Beijing, 100083, the People's Republic of China

ARTICLE INFO

Article history:
Received 16 March 2022
Received in revised form
29 October 2022
Accepted 1 November 2022
Available online 5 November 2022

Edited by Yan-Hua Sun

Keywords:
Modified carbon black nanoparticles
Interfacial tension reduction
Displacement efficiency
Synergistic effects
Enhanced oil recovery

ABSTRACT

A novel nanofluid of modified carbon black (MCB) nanoparticles was initially developed for enhanced oil recovery (EOR) in low permeability reservoirs. The MCB nanoparticles were obtained via a three-step reaction involving modification by oxidation, acyl chlorination, and activated grafting. MCB nanoparticles were spherically dispersed, with an average size of 72.3 nm. Compared with carbon black (CB) nanoparticles, dispersed MCB nanoparticles can effectively reduce the oil–water interfacial tension (IFT) to 10^{-2} mN/m and change the surface wettability of sand particles. Based on the results of core flooding experiments, the MCB nanoparticles exhibited a better EOR capacity than surfactants and CB nanoparticles, and the final oil recovery was significantly increased by 27.27%. The core scanning test showed that the MCB nanoparticles could plug high permeability channels by adsorbing onto the surfaces of sand particles and forming larger aggregates that bridge across pores or throats, resulting in a higher swept volume. The synergistic effects of improved swept volume and oil displacement efficiency were the EOR mechanisms of the MCB nanoparticles. The studies indicate that these MCB nanoparticles have excellent potential for EOR in low permeability reservoirs.

1. Introduction

To date, most conventional oilfields across the globe have entered a middle-late period of production, which has resulted in inevitable and important changes in production concerning conventional reservoirs. The exploration and development of conventional oil reservoirs have shifted to low permeability, ultralow permeability, heavy oil, shale oil, and other unconventional oil and gas reservoirs (Aguilera and Ripple, 2012; Salameh, 2003; Wang et al., 2016). Low permeability reservoirs have become an important petroleum resource in recent years (Holditch, 2013; Jiao, 2019; Mayol et al., 2020). However, the unique characteristics of low permeability, low porosity, and high injection pressure make oil recovery difficult in these reservoirs. Considering enhanced oil recovery techniques, nanomaterials have emerged as important agents in low permeability reservoirs (Delamaide et al., 2014; Chung et al., 2017; Negin et al., 2016; Rezk and Allam, 2019).

As an emerging technology, nanomaterials have broad prospects in the life sciences, electronics, medicine, and other fields (Chen and Chatterjee, 2013; Hussain, 2018; Yao et al., 2014). Nanomaterials are within the mesoscopic system, defined as being situated between the macroscopic scale of objects and the microscopic scale of particles, and have unique physical and chemical properties, including small size effects, surface effects, and macroscopic quantum effects (Du et al., 2010; Moon et al., 2011; Worthen et al., 2016). Thus, the compounding and modification technology of nanomaterials has been proposed for the EOR treatments in oilfields (Mariyate and Bera, 2022; Bera and Belhaj, 2016). Compared with the mechanisms underlying conventional chemical flooding systems (alkali flooding, surfactant flooding, polymer flooding, etc.), the mechanisms involving nanofluids are more complex (Gbadamosi et al., 2018; Kamkar et al., 2020; Khaleduzzaman et al., 2013; Sharma et al., 2016; Zhao et al., 2018a; Bera et al., 2015; Mariyate and Bera, 2021). These mechanisms include conventional mechanisms such as profile control and low interfacial tension (IFT) and take into account the unique characteristics of nanoparticles, which have promising application potential for EOR in low permeability reservoirs. Previous studies

* Corresponding author.
E-mail address: zhaoguang@upc.edu.cn (G. Zhao).

https://doi.org/10.1016/j.petsci.2022.11.003

have shown that a reduction in the oil–water IFT, changes in the surface wettability of sand particles, and the structural disjoining pressure are the main factors responsible for oil displacement mechanisms in nanofluids. In addition, nanofluids can also obviously enhance the oil displacement efficiency when combined with other oil displacement agents (Bera et al., 2020). Among the numerous nanofluid EOR technologies, modified silica and graphene-based nanosheets are the most widely studied in low permeability reservoirs (Al-Anssari et al., 2016; Gomari et al., 2019; Kamkar et al., 2017, 2020; Luo et al., 2016, 2017; Radnia et al., 2018). Although these nanofluids have shown excellent application potential, the rigidity of modified silica and the high cost of graphene-based nanosheets limit their oilfield applications. Due to their rigidity, modified silica particles cannot deform upon passing through small throat holes in low permeability reservoirs. These silica particles can enter only large pores or cracks, but oil rarely remains in these regions, which leads to low oil recovery (Nguele et al., 2019; Sun et al., 2017). Moreover, low concentrations of graphene-based nanosheets have exhibited high performance, which indicates the potential of graphene-based nanosheets in oilfield applications. However, the cost of graphene-based nanosheets is high, and the industrialized production of these materials remains a technical bottleneck.

To overcome the problems associated with the above-mentioned nanofluids, a novel nanofluid containing MCB nanoparticles was prepared and used for EOR treatment in low permeability reservoirs. CB nanoparticles have been used in various fields (as conductive materials, rubber-reinforced materials, dyes, etc.) because of their excellent properties (Huang et al., 2021; Raju et al., 2022; Qiu et al., 2021). CB nanoparticles have the excellent characteristics of low cost, nanometer-scale size, softness, self-lubrication, thermal stability, and ease of modification (Long et al., 2013; Probst and Grivei, 2002; Toupin and Bélanger, 2007). These characteristics make them promising for use in low permeability reservoirs. However, the unmodified CB nanoparticles easily form irreversible aggregates in nanofluid solutions, which is not conducive to their injection into target reservoirs. Previous reports have shown that functional groups such as hydroxyl or carboxyl groups are present on the surfaces of oxidized CB nanoparticles, which enhances the reactivity of these nanoparticles (Han et al., 2017; Papirer et al., 1991). However, these functional groups are usually not very reactive, so they need to be transformed into groups with higher reactivity (via oxidation activation). The carboxyl groups present on the surfaces of oxidized CB nanoparticles can react with thionyl chloride to form acyl chloride groups, and these acyl chloride groups can subsequently react with surfactants containing hydroxyl groups, which allows other molecules to be grafted onto the surfaces of these nanoparticles (Fujiki et al., 1990; Tsubokawa et al., 1989). In this study, MCB nanoparticles were designed and prepared via a three-step reaction involving modification by oxidation, acyl chlorination, and activated grafting. The morphology, dispersed stability, IFT reduction capacity, wettability alteration capacity, and potential EOR capacity of the MCB nanoparticles were systematically studied. In addition, the distribution of the MCB nanoparticles in porous media was determined to elucidate the EOR mechanism. Through this study, we hope that MCB nanoparticles will be promising chemical agents for EOR treatment in low permeability reservoirs.

2. Materials and methods

2.1. Experimental materials

CB nanoparticles were purchased from Tianjing Yiborui Chemical Co., Ltd., China. Thionyl chloride ($SOCl_2$, analytical grade), toluene (C_7H_8, analytical grade), triethylamine ($C_6H_{15}N$, 99 wt%), and dibutyltin dilaurate ($C_{32}H_{64}Sn$, analytical grade) were provided by Shanghai Aladdin Biochemical Technology Co., Ltd., China, and tetradecyl hydroxypropyl sulfobetaine (THSB, $C_{19}H_{41}O_4NS$, 60 wt%) surfactant was obtained from Zhengzhou Yihe Fine Chemicals Co., Ltd, China. Crude oil with a density of 0.76 g/cm^3 and a viscosity of 1.09 mPa s was provided by the Zhuang 211 Block of Changqing Oilfield in China. The salinity of the simulated water of Zhuang 211 Block was 33,598 mg/L (Na^++K^+, 11790 mg/L; Ca^{2+}+Mg^{2+}, 1,283 mg/L; Cl^-, 20,300 mg/L; HCO_3^-, 122 mg/L; CO_3^{2-}, 55 mg/L; SO_4^{2-}, 44 mg/L). The simulated water was used to evaluate the performance of MCB nanoparticles at 59.6 °C under the Zhuang 211 Block condition.

2.2. Design and synthesis of MCB nanoparticles

Three steps of oxidation, acylation, and activated grafting were used to synthesize MCB nanoparticles. First, carboxyl groups were generated on the surfaces of the MCB nanoparticles via oxidation reactions. Second, the carboxyl groups were converted into more reactive acyl chloride groups by acylation. Third, the acyl chloride groups easily reacted with the hydroxyl groups on a surfactant, and the surfactant was grafted onto the surfaces of CB nanoparticles. The molecular design process for the MCB nanoparticles is shown in Figs. 1–3. The specific reactions involved in preparing the MCB nanoparticles are as follows.

For the oxidation step, 10 g of CB nanoparticles were dispersed in 100 g of HNO_3 with a concentration of 40 wt%; the mixture was ultrasonically dispersed for 20 min at room temperature so that it was uniform. Next, oxidation was carried out in an 80 °C oil bath, under continuous stirring for 5 h. Then, the reaction solution was filtered and washed with deionized water three times to obtain oxidized CB nanoparticles.

For the acylation step, 10 g of the product from the first step, 2.5 g of $SOCl_2$, and 0.2 g of $C_6H_{15}N$ were added sequentially to 100 g of toluene; the mixture was ultrasonically dispersed for 20 min in an ice bath. Then, the reaction was allowed to continue at 70 °C for 4 h. After the reaction was complete, toluene and unreacted $SOCl_2$ in the solution were removed by rotary evaporation at 80 °C. Acyl chloride-containing CB nanoparticles were obtained after the reaction.

For the activated grafting step, 10 g of the product from the second step and 5 g of the THSB surfactant were added sequentially to 100 g of toluene; the mixture was ultrasonically dispersed for 20 min at room temperature. Then, 0.2 g of $C_{32}H_{64}Sn$ as a catalyst was added, and the solution was heated at 65 °C for 4 h to allow the reaction to proceed. Subsequently, the obtained product was washed four times with water and then dried in a rotary evaporator at 80 °C. Finally, MCB nanoparticles were obtained by grinding.

2.3. Characterization of the MCB nanoparticles

Fourier transform infrared (FT-IR) spectroscopy (VERTEX 70 FT-IR spectrometer) was used to examine the MCB nanoparticles. The morphology of the MCB nanoparticles was observed via transmission electron microscopy (TEM) (JEOL JEM-2100, JEOL Ltd., Japan). A laser particle size analyzer (NanoBrook Omni, Brookhaven Instruments Corporation, Holtsville, NY) was used to evaluate the stability of the MCB nanoparticles. The oil–water IFT was determined using a TX-500C spinning drop interfacial tensiometer. The wettability of glass slides was determined by measurement of the contact angle using a JC2000D contact angle measuring instrument (Shanghai Zhongchen Digital Technology Equipment Co., Ltd., China).

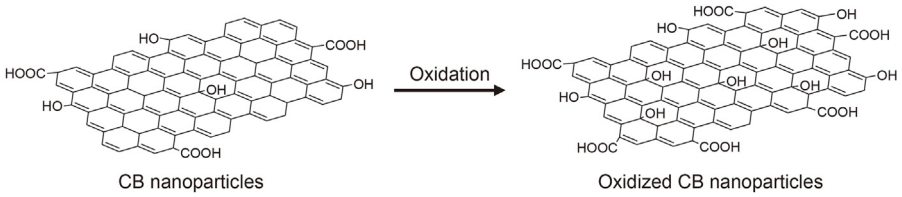

Fig. 1. Molecular design involved in the oxidation process.

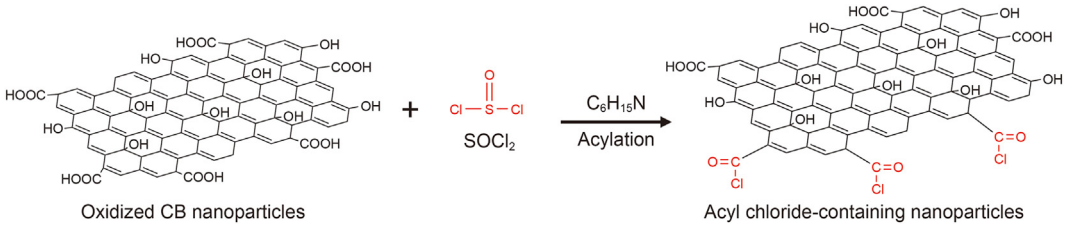

Fig. 2. Molecular design involved in the acyl chlorination process.

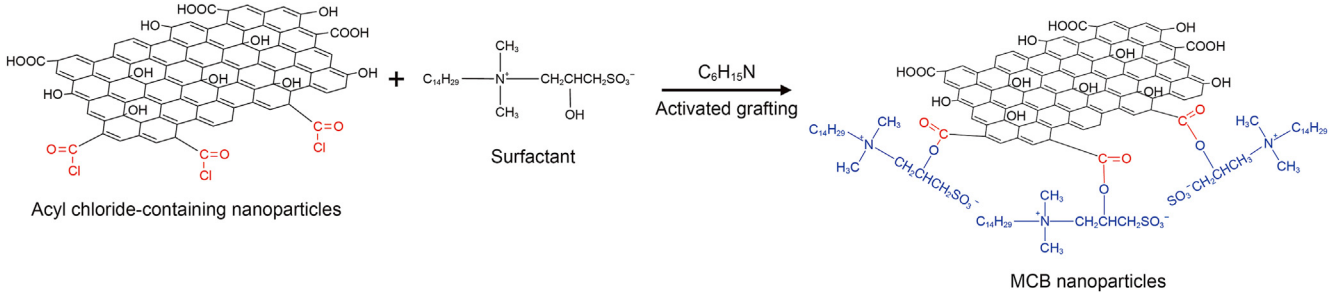

Fig. 3. Molecular design involved in the activated grafting process.

2.4. Preparation of the MCB nanofluids

MCB nanoparticles were added to simulated water, and the solution was stirred for 5 min at room temperature to obtain MCB nanofluids.

2.5. Preparation of glass slides with different wettability

Glass slides with a length of 5 cm and a width of 2 cm were soaked in concentrated sulfuric acid and hydrogen peroxide solution for 3 h, then rinsed with deionized water repeatedly and dried at 130 °C; finally, the water-wetting glass slides were obtained. The dried water-wetting glass slides were placed in the paraffin system and aged at 130 °C for 7 days to obtain oil-wetting glass slides. Oil-wetting glass slides with an initial contact angle of 115.2° and water-wetting glass slides with an initial contact angle of 10.6° were used to investigate the wettability of the MCB nanoparticles. The oil-wet and water-wet glass slides were placed in the MCB nanoparticle nanofluid and aged for different days. Then the contact angle of these two systems was determined. The concentration of the MCB nanoparticles and temperature were 0.25 wt% and 59.6 °C, respectively.

2.6. Potential EOR capacity of the MCB nanoparticles

The potential EOR capacity of the surfactant, CB nanoparticles, and MCB nanoparticles was evaluated by core flooding models (Fig. 4). The permeability of core samples is 0.23 mD, corresponding to the matrix permeability. However, there were artificial cracks within the core samples, and the permeability of the whole core sample was about 21 mD due to the high connectivity in the cracks. The physical properties of cores were shown in Table 1.

First, three cores were successively saturated with simulated water and crude oil. Then, water was introduced until the produced water rate reached 98%. Subsequently, these three cores were respectively injected with 1 pore volume (PV) of surfactant, CB nanoparticle, and MCB nanoparticle dispersion solutions. Finally, water was reintroduced until the produced water rate reached 98%. For this process, the injection concentration of MCB nanoparticles and injection speed of the pump were set to 0.25 wt% and 0.2 mL/min, respectively.

All experimental conditions were conducted under the conditions at Zhuang 211 Block of Changqing Oilfield in China, and the core flooding experimental temperature was set at 59.6 °C. The pressure and produced fluid were recorded to evaluate the potential EOR capacity of the MCB nanoparticles. The resistance factor was calculated with Eq. (1):

$$F_R = \frac{k_i}{k_o} \tag{1}$$

where F_R is the resistance factor; k_o is the original permeability of the core; and k_i is the permeability of the MCB nanoparticle injection stage and water flooding stage.

2.7. Distribution of the MCB nanoparticles in porous media

The distribution of the surfactant and MCB nanoparticles in

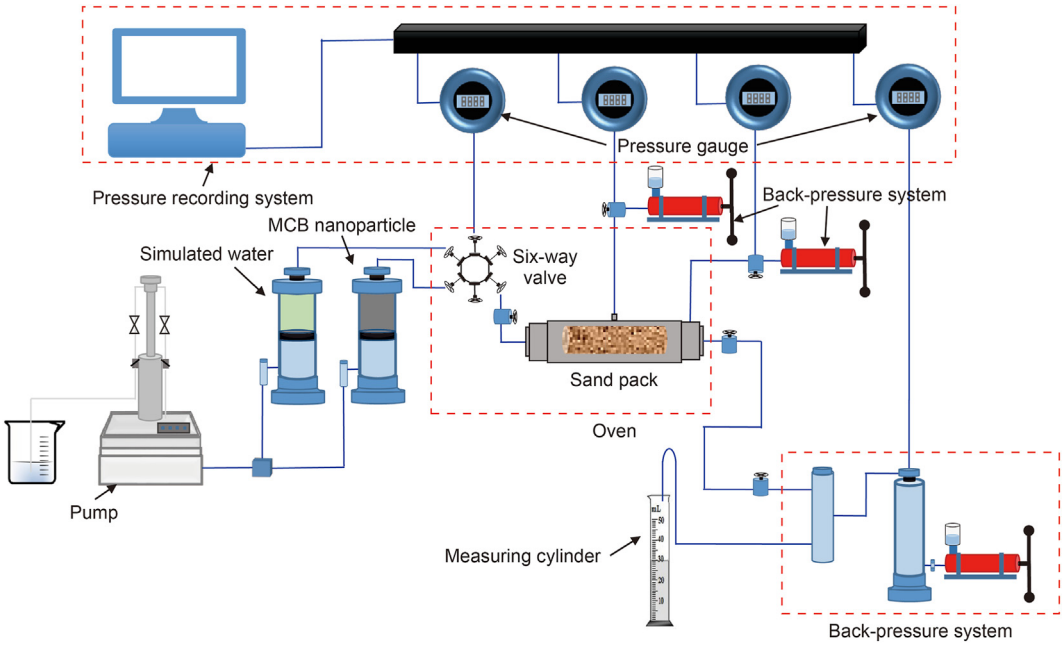

Fig. 4. Schematic depicting the core flooding model.

Table 1
Displacement effects of the surfactant, CB nanoparticles and MCB nanoparticles.

System	Permeability, mD	Length, mm	Diameter, mm	Pore volume, mL	Oil saturation, %	Water flooding recovery, %	Final recovery, %	Increased recovery, %
Surfactant	21.7	101	25	7.66	76.02	49.30	60.56	11.26
CB nanoparticles	20.9	100	25	7.39	77.12	52.78	67.92	15.14
MCB nanoparticles	21.2	100	25	7.52	77.05	49.65	76.92	27.27

porous media was analyzed and compared. First, 1 PV of the above two dispersion solutions was injected into the cores and then aged at 59.6 °C for 7 days. Then, the cores were freeze-dried for 20 h in a vacuum freeze dryer. Finally, 5–10 mm fragments were cut from the middle of the cores and imaged with a Hitachi S-4800 scanning electron microscope (SEM, Hitachi High Technologies corporation, Japan).

3. Results and discussion

3.1. Characterization of the MCB nanoparticles by FT-IR

Fig. 5 shows the FT-IR spectra of the CB nanoparticles, acyl chloride-containing CB nanoparticles, and MCB nanoparticles. As shown by the blue curve (attributed to the CB nanoparticles), characteristic peaks were observed at 1107, 1464, and 1745 cm^{-1}; which were assigned to C–O stretching vibrations, symmetric C–H deformation vibrations in methyl groups, and C=O stretching vibrations in carboxylic groups, respectively. The strong signals at 2854 and 2932 cm^{-1} were attributed to symmetric and asymmetric C–H stretching vibrations of methyl groups. After modification with HNO_3 and $SOCl_2$, the spectrum of the acyl chloride-containing CB nanoparticles (black curve) exhibited new peaks at 813 and 3329 cm^{-1}, and these peaks were assigned to C–Cl stretching and O–H stretching, respectively. These features indicate that the surfaces of the CB nanoparticles were successfully oxidized and modified with $SOCl_2$ molecules. In the MCB nanoparticle spectrum (red curve), a strong characteristic peak was observed at 1182 cm^{-1}, and was attributed to S=O stretching vibrations of the sulfonate moiety. In addition, a peak at 1378 cm^{-1} was observed and attributed to –N+–C–H deformation vibrations in quaternary ammonium groups. These results indicate that the THSB surfactant was successfully grafted onto the CB nanoparticles. Therefore, MCB nanoparticles with active groups were successfully prepared.

3.2. Morphology of the MCB nanoparticles

Fig. 6 presents representative TEM images of the CB nanoparticles and MCB nanoparticles in deionized water. Large aggregates were clearly observed in the CB nanoparticle system (Fig. 6a and b), while the MCB nanoparticles were less agglomerated (Fig. 6d and e). The average sizes of the CB nanoparticles and MCB nanoparticles were 184.7 and 72.3 nm, respectively (Fig. 6c and f). This indicates that the degree of aggregation was obviously reduced after modification. The high surface energy of CB nanoparticles hinders their uniform dispersion in water (Hwang et al., 2018; Soares et al., 2014). However, the surface energy was lower after the surfactant was grafted onto the surfaces of the CB nanoparticles, leading to the nanoparticles being less agglomerated (Alexander et al., 2016; Maurya et al., 2017). Additionally, there were quaternary ammonium groups and sulfonate groups on the surfaces of the MCB nanoparticles, which improved their wettability in water and led to improved dispersion.

3.3. IFT reduction capacity of the MCB nanoparticles

The grafted surfactant has the following two functions: (1) it allows stable MCB nanoparticle dispersions to be formed, and (2) it reduces the oil–water IFT in porous media. Therefore, the IFT reduction capacity of the surfactant and the MCB nanoparticles was

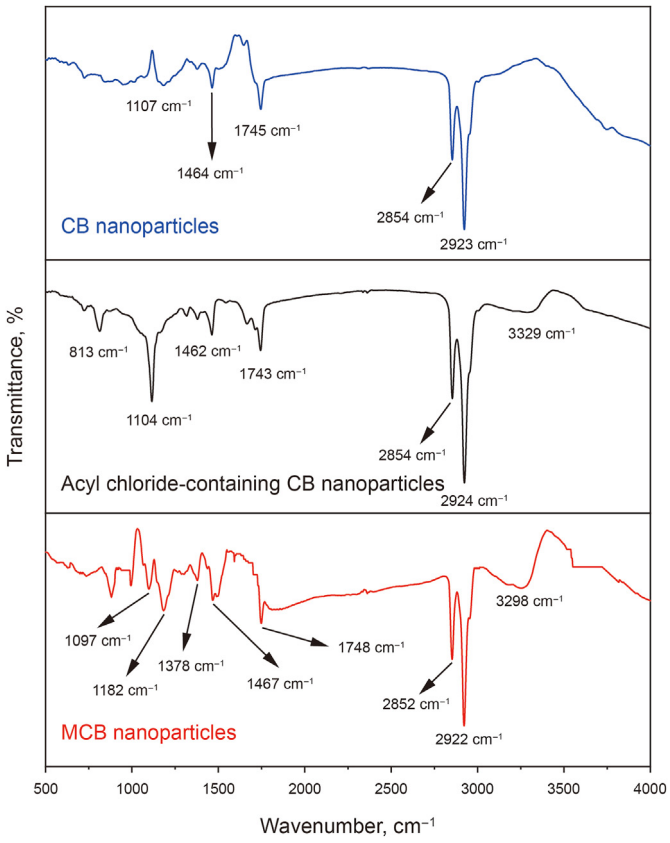

Fig. 5. FT-IR spectra of the CB nanoparticles, acyl chloride-containing CB nanoparticles, and MCB nanoparticles.

investigated under Zhuang 211 Block conditions. Fig. 7a shows that the oil–water IFT of these two systems decreased with increasing concentration. The surfactant exhibited an obvious IFT reduction capacity, and the MCB nanoparticles can reduce the IFT from 0.1 to 0.02 mN/m when the concentration was increased from 0.1 wt% to 0.25 wt%. This could be due to the grafted surfactant allowing the MCB nanoparticles to adsorb more easily at the oil–water interface, which endows the nanoparticles with an enhanced ability to reduce the oil–water IFT. However, the active groups of the MCB nanoparticles were less abundant than those in the THSB surfactant system at the same concentration. Therefore, the IFT reduction capacity of the MCB nanoparticles was lower than that of the THSB system. With increasing aging time, the IFT of these two systems increases, and the final IFT of the MCB nanoparticles was in the range of 10^{-1} to 10^{-2} mN/m after 80 days (Fig. 7b). This indicates that long-term aging has a slight effect on the ability of these two systems to reduce the IFT. The quaternary ammonium cations and sulfonic acid anions in the THSB surfactant system endow the surfactant with good heat and salt resistance. Therefore, both the THSB surfactant system and the MCB nanoparticles can effectively reduce the IFT after long-term aging under reservoir conditions.

3.4. Wettability of the MCB nanoparticles

Due to hydrogen bonding and van der Waals forces interactions, the adsorption of MCB nanoparticles on sand particles is inevitable. The adsorption behavior affects the wettability of the surfaces of sand particles, thus affecting the displacement effect of MCB nanoparticles. The contact angle observed for these two glass slides was measured after the slides were aged in the MCB nanoparticle dispersion solution. Changes in the contact angle as a function of aging time are shown in Fig. 8.

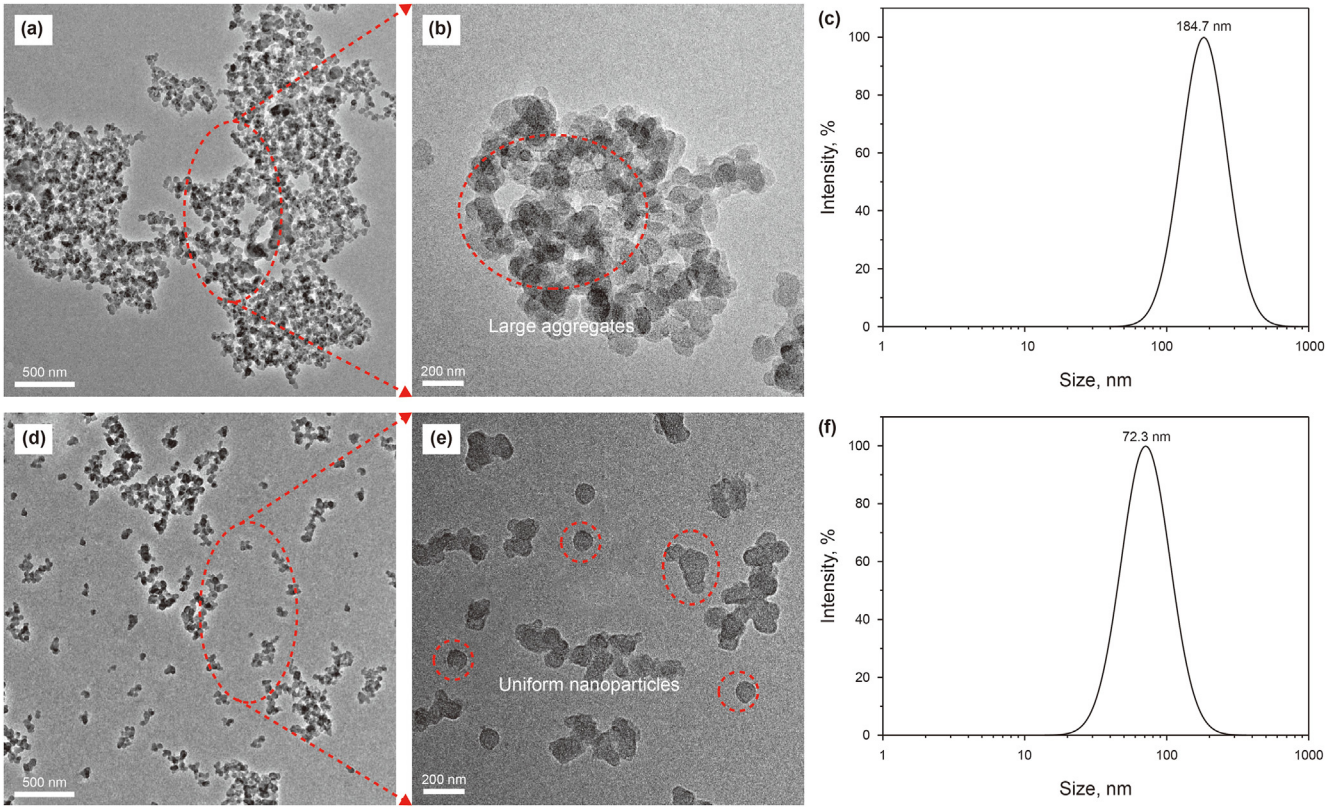

Fig. 6. TEM images and particle size distribution of the CB nanoparticles (**a**, **b**, **c**) and MCB nanoparticles **(d, e, f).**

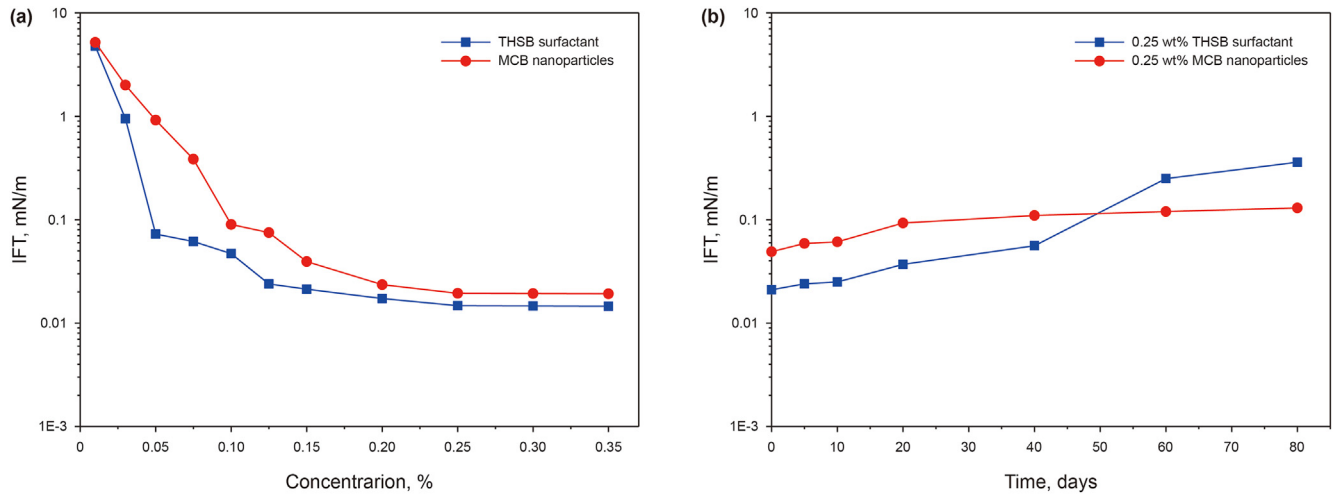

Fig. 7. IFT reduction capacity of the surfactant and MCB nanoparticles: (**a**) IFT at different concentrations; (**b**) IFT as a function of aging time.

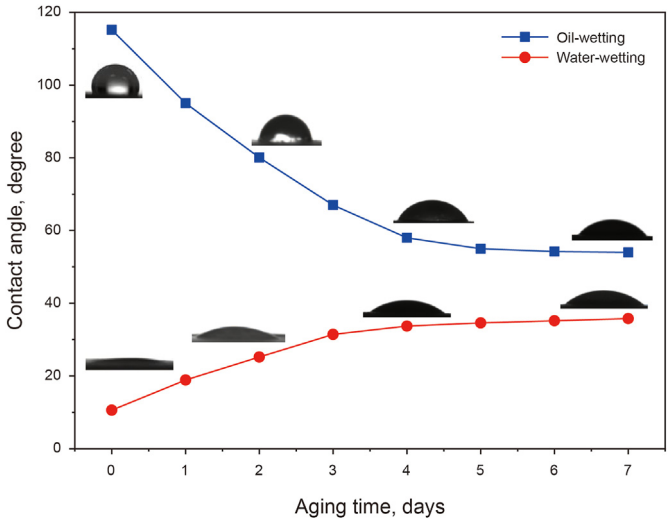

Fig. 8. Changes in contact angle as a function of aging time.

As shown in Fig. 8, the MCB nanoparticles changed the wettability of the glass slides with increasing aging time. After aging for 7 days, the contact angle of the oil-wetting slide decreased from 115.2° to 54.1°, while the contact angle of the water-wetting slide increased from 10.6° to 35.8°. When the surfactant was grafted onto the CB nanoparticles, the MCB nanoparticles became active and could adsorb on the glass surface, forming a stable adsorption film. Thus, the wettability of the glass slide surfaces significantly changed after the slides were soaked in the MCB nanoparticle dispersion solution. Due to interactions of hydrogen bonding and van der Waals forces, the MCB nanoparticles could rapidly occupy the adsorption sites of the glass slide surfaces during the initial stage (0–4 days); then, the contact angle obviously changed, resulting in changes in the wettability of the two glass slides. With increasing aging time, the contact angle for the glass slides remained nearly unchanged. The oil-wetting glass slides became water-wetting glass slides, and the strong water-wetting glass slides became weak water-wetting glass slides. The adsorption behavior of the MCB nanoparticles on the glass slide surfaces involved the dynamic, equilibrium processes of adsorption and desorption (Saini et al., 2019). The adsorption behavior of the MCB nanoparticles was affected not only by their inherent properties but also by the wettability of the glass slide. With the aggregation of a few MCB nanoparticles, the adsorption sites on the glass slides decreased the adsorption of the MCB nanoparticles on the slide surface; thus, the wettability of the glass slides remained essentially unchanged. When the wettability of a rock surface changes, crude oil can be easily stripped from the rock surface. Therefore, when the displacement effect of MCB nanoparticles is improved, oil recovery will be enhanced.

3.5. Stability of the dispersed MCB nanoparticles

Excellent stability is a key feature of nanoparticles used for EOR treatment. In this section, changes in particle size and zeta potential were used to characterize the stability of dispersed CB nanoparticles and MCB nanoparticles. The nanoparticle concentration and experimental temperature were 0.25 wt% and 30 °C, respectively. The pH value of the CB nanoparticle dispersion solution was 8.1 while that of the MCB nanoparticle dispersion solution was 5.9.

As shown in Fig. 9a, the initial zeta potential of the CB nanoparticles was −14.8 mV, while that of the MCB nanoparticles was −35.6 mV. Based on our understanding, 30 mV is regarded as the critical zeta potential value of a stable dispersion. The results indicate that the dispersed MCB nanoparticles are more stable than the dispersed CB nanoparticles. Additionally, the initial average particle size of the CB nanoparticles was 184.7 nm, while that of the MCB nanoparticles was 72.3 nm. With increasing aging time, the zeta potential and particle size of the MCB nanoparticles remained nearly unchanged. In contrast, the zeta potential and particle size of the CB nanoparticles were obviously increased. After aging for 80 days, a large number of CB nanoparticles aggregated to form large agglomerates, and the particle size reached nearly 10 μm, leading to an unstable nanoparticle system. The aggregation behavior of these CB nanoparticles is related to their larger surface area, smaller particle size, high surface energy, and complex surface structure. When the surfactant was grafted onto the nanoparticles, the presence of tetradecyl sulfobetaine group on the surfaces of the CB nanoparticles enhanced the electrostatic repulsion and steric hindrance between the MCB nanoparticles (Xue et al., 2016). Thus, these actions led to the MCB nanoparticle dispersions being stable in water.

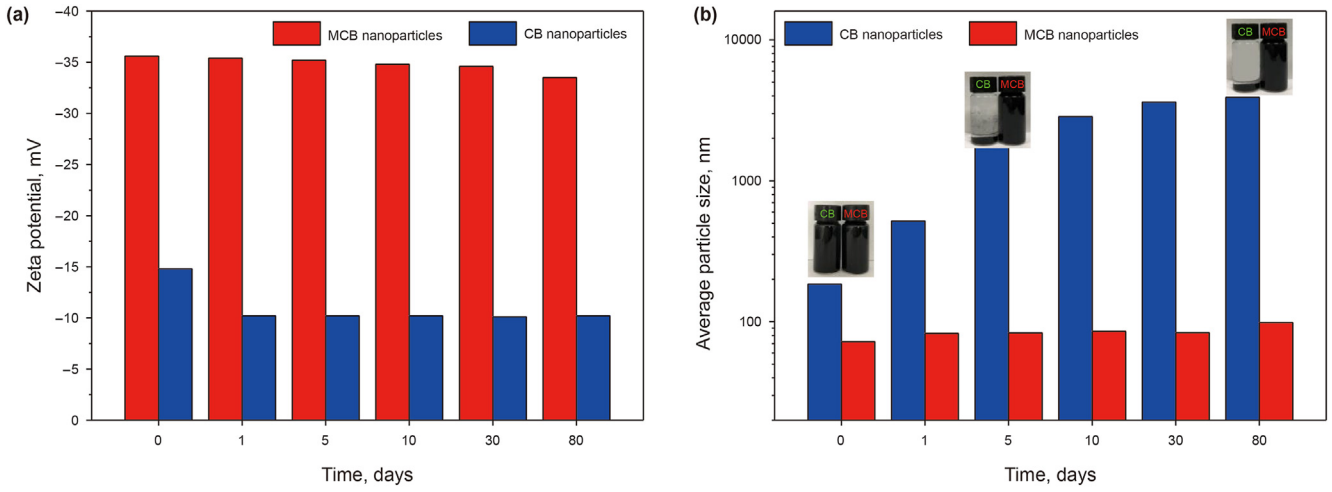

Fig. 9. Zeta potential and particle size distribution of the CB and MCB nanoparticles as a function of aging time: (**a**) zeta potential; (**b**) particle size distribution.

3.6. Potential EOR capacity of the MCB nanoparticles

Table 1 shows the potential EOR capacity of the surfactant, CB nanoparticles, and MCB nanoparticles. The injection of the above three systems can effectively increase the recovery rate by more than 10%. The experimental results indicate that all three systems can enhance oil recovery, but the EOR capacities are significantly different during the injection stage. The EOR capacity of the MCB nanoparticles is significantly higher than the EOR capacities of the surfactant and CB nanoparticles. This indicates that the injection of MCB nanoparticles has great EOR potential in low permeability reservoirs.

Figs. 10–12 shows the water cut, oil production, and pressure curves obtained during surfactant, CB nanoparticle, and MCB nanoparticle displacement. A dominant flow channel is formed after a long-term water flooding, resulting in a decrease in the injection pressure and an invalid water flooding cycle. When the surfactant, CB nanoparticles, and MCB nanoparticles were injected, they preferentially entered high-permeability zones or cracks under the injection pressure. Since the surfactant cannot change the water-oil mobility ratio or improve the formation profile, the injected surfactant is easily channeled through the high permeability zones or cracks, reducing the displacement effect and

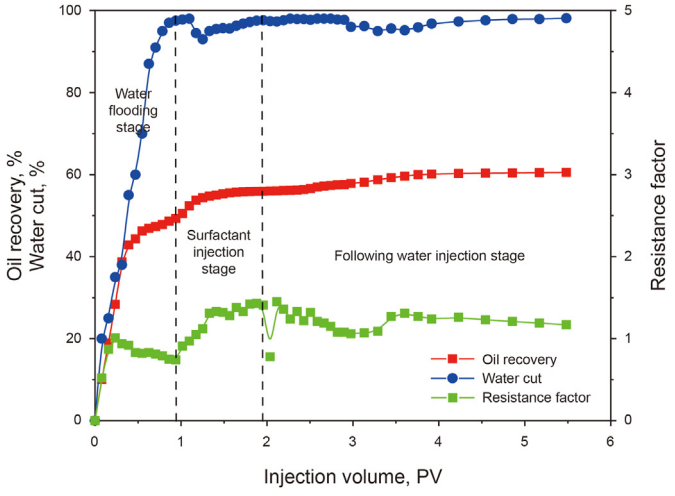

Fig. 10. Oil recovery, water cut, and resistance factor of the surfactant.

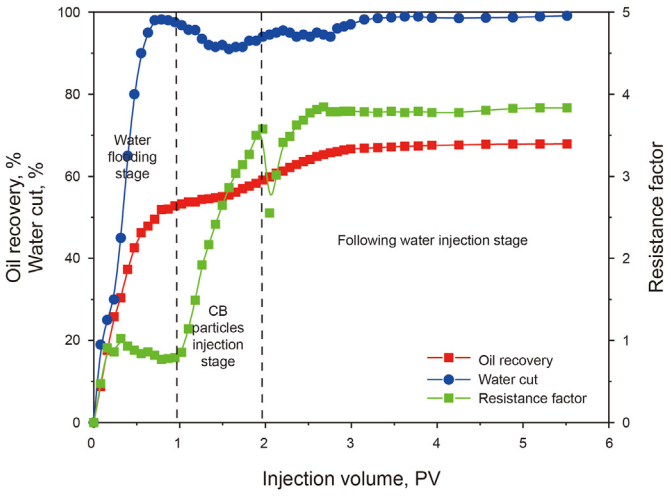

Fig. 11. Oil recovery, water cut, and resistance factor of the CB nanoparticles.

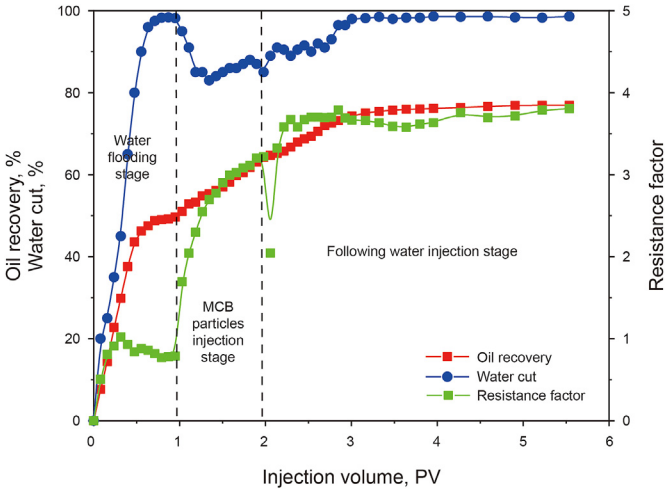

Fig. 12. Oil recovery, water cut, and resistance factor of the MCB nanoparticles.

recovery efficiency. The oil was enhanced, which is mainly due to contact with the remaining oil in the high-permeability zones. However, there was still a considerable amount of oil remaining in the middle and low permeability zones that could not be driven out during the injection process. Moreover, the injected surfactant could not effectively control the high-permeability zone or cracks, so the subsequently injected water continued to channel along the high-permeability zones, resulting in a decrease in the injection pressure. When CB nanoparticles were injected into the core, they adsorbed on the surfaces of the sand particles, formed larger aggregates, and bridged pores or throats, so the formation profile could be effectively adjusted. Thus, the subsequently introduced water was diverted to the upswept areas of the middle- and low-permeability zones, and the remaining oil was driven out. However, due to their weak stability in the dispersion solution, CB nanoparticles were easily retained in the near-wellbore zone, and it was difficult for them to enter the deep formation zone. The stably dispersed MCB nanoparticles could easily enter the deep formation zone; thus, the formation profile was effectively improved. Additionally, due to the surfactant being grafted on the nanoparticle surfaces, the MCB nanoparticles were able to reduce the oil–water IFT, and the remaining oil in the middle- or low-permeability zones could be easily driven out. The synergistic effects of improved swept volume and oil displacement efficiency indicate that the EOR capacity of the MCB nanoparticles was better than the EOR capacities of the surfactant and CB nanoparticles (Rezvani et al., 2020; Zhao et al., 2018b).

3.7. Distribution of the MCB nanoparticles in porous media

Fig. 13 shows representative SEM images of the surfactant and MCB nanoparticles distributed in porous media. However, the distributions of the surfactant and MCB nanoparticles significantly differ. As shown in Fig. 13a–c, large pores and cracks remained after the surfactant was injected. This indicates that the surfactant system can hardly improve the formation profile, leading to injected surfactant channeling along the high permeability channels or cracks. The oil was enhanced, which is mainly due to the surfactant contacting with remaining oil in the high permeability zones, and a large amount of remaining oil in the middle and low permeability zones could not be driven out. Therefore, the EOR capacity of the surfactant was lower than the EOR capacities of the CB and MCB nanoparticles.

In contrast to observe for the surfactant, when the MCB nanoparticles were injected into the formation zone, the nanoparticles could be deformed and easily enter the deep formation zone due to their soft characteristics and nanometer-scale size. When flowing in large pores or throats, the MCB nanoparticles could be adsorbed on the surfaces of sand particles via hydrogen bonding or van der Waals force interactions (Fig. 13d, g). The adsorption of the MCB nanoparticles reduced the effective flow radius of these pores and throats. When the size of the MCB nanoparticles was slightly smaller than the pore throat radius, several MCB particles can easily be aggregated to form larger agglomerates that bridge across these pores and throats, resulting in the formation of an effective plugging layer (Fig. 13e, h). In addition, the MCB nanoparticles could

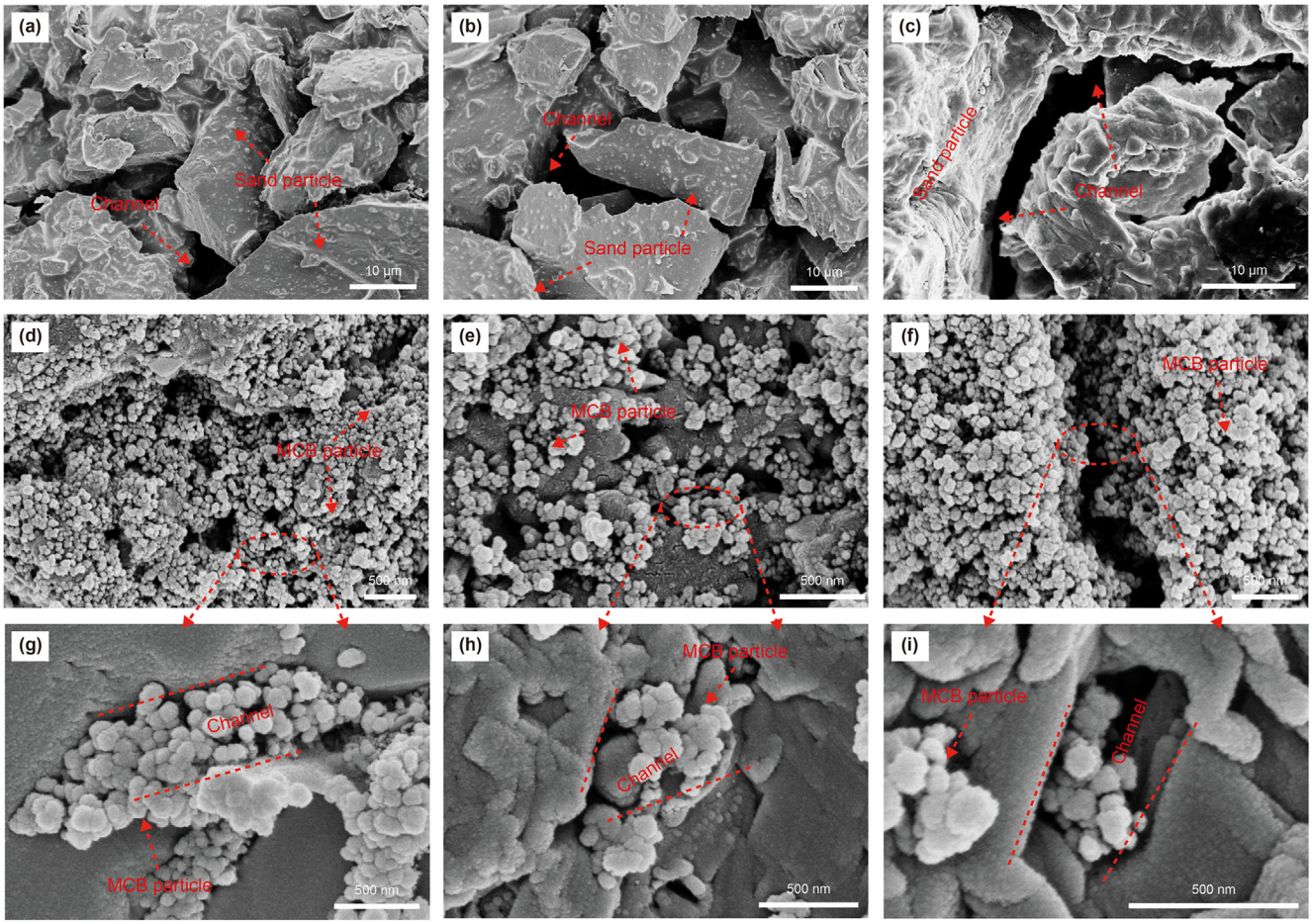

Fig. 13. Morphology of the surfactant and MCB nanoparticles in porous media: (**a**, **b**, **c**) surfactant system and (**d**, **e**, **f**, **g**, **h**, **i**) MCB nanoparticles.

also be adsorbed or aggregate in the fracture channels (Fig. 13f, i); thus, the size of the fracture channels decreased. Through adsorption, aggregation, and bridging in porous media, the MCB nanoparticles exhibited good profile control and displacement ability. The injected water could be forced to the middle or low permeability zones; thus, the swept volume was increased. Additionally, due to the surfactant being grafted on the MCB nanoparticles, this system underwent displacement mechanisms that are similar to those of the surfactant. When the MCB nanoparticles contacted the remaining oil in the high permeability zones, the nanoparticles adsorbed at the oil–water interface and reduced the oil–water IFT (Maurya and Mandal, 2018; Rezvani et al., 2019). Moreover, the adsorbed MCB nanoparticles also altered the wettability of the surfaces of sand particles. Consequently, the remaining oil could be easily driven out; oil recovery was definitely enhanced after the injection of the MCB nanoparticles.

4. Conclusions

In this work, MCB nanoparticles were developed as novel chemical agents and exhibited excellent potential for EOR treatment in low permeability reservoirs. MCB nanoparticles were obtained via oxidation of CB nanoparticles, acyl chlorination, and grafting of active groups. The MCB nanoparticles had properties similar to those of the grafted surfactant which could reduce oil–water IFT and altered the wettability of the surfaces of sand particles. The MCB nanoparticles had a better and more stable dispersion capacity than conventional CB nanoparticles, which allowed the MCB nanoparticles to enter the deep formation zone. After being adsorbed on the surfaces of sand particles, the MCB nanoparticles formed larger aggregates and bridged across pores and throats; so the MCB nanoparticles effectively plugged the high-permeability channels and diverted the introduced water into unswept zones. In addition, the MCB nanoparticles had properties that were similar to those of the surfactant, indicating that they can easily drive out oil remaining in the high-permeability zones. Therefore, the EOR capacity of the MCB nanoparticles was greatly improved. These results confirm that the injection of MCB nanoparticles is an effective EOR treatment in low permeability reservoirs.

Declaration of competing interest

The article is original. The article has been written by the stated authors who are all aware of its content and approve its submission. The article has not been published previously. The article is not under consideration for publication elsewhere. No conflict of interest exists. If accepted, the article will not be published elsewhere in the same form, in any language, without the written consent of the publisher.

Acknowledgments

This work was supported by the National Key R&D Program of China (2018YFA0702400) and National Natural Science Foundation of China (5207040347).

References

Aguilera, R.F., Ripple, R.D., 2012. Technological progress and the availability of European oil and gas resources. Appl. Energy 96, 387–392. https://doi.org/10.1016/j.apenergy.2012.02.069.

Al-Anssari, S., Barifcani, A., Wang, S., et al., 2016. Wettability alteration of oil-wet carbonate by silica nanofluid. J. Colloid Interface Sci. 461 (1), 435–442. https://doi.org/10.1016/j.jcis.2015.09.051.

Alexander, S., Eastoe, J., Lord, A.M., et al., 2016. Branched hydrocarbon low surface energy materials for superhydrophobic nanoparticle derived surfaces. Acs. Appl. Mater. Inter. 8 (1), 660–666. https://doi.org/10.1021/acsami.5b09784.

Bera, A., Belhaj, H., 2016. Application of nanotechnology by means of nanoparticles and nanodispersions in oil recovery - a comprehensive review. J. Nat. Gas Sci. Eng. 34, 1284–1309. https://doi.org/10.1016/j.jngse.2016.08.023.

Bera, A., Mandal, A., Kumar, T., et al., 2015. The effect of rock-crude oil-fluid interactions on wettability alteration of oil-wet sandstone in the presence of surfactants. Petrol. Sci. Technol. 33 (5), 542–549. https://doi.org/10.1080/10916466.2014.998768.

Bera, A., Shah, S., Shah, M., et al., 2020. Mechanistic study on silica nanoparticles-assisted guar gum polymer flooding for enhanced oil recovery in sandstone reservoirs. Colloid. Surface. 598, 124833. https://doi.org/10.1016/j.colsurfa.2020.124833.

Chen, A., Chatterjee, S., 2013. Nanomaterials based electrochemical sensors for biomedical applications. Chem. Soc. Rev. 42 (12), 5425–5438. https://doi.org/10.1039/C3CS35518G.

Chung, L.H., Meng, Y., Quoc, N., 2017. Nanotechnology for oilfield applications: challenges and impact. J. Petrol. Sci. Eng. 157, 1160–1169. https://doi.org/10.1016/j.petrol.2017.07.062.

Delamaide, E., Tabary, R., Rousseau, D., 2014. Chemical EOR in low permeability reservoirs. SPE EOR Conference at Oil and Gas West Asia. https://doi.org/10.2118/169673-MS.

Du, K., Glogowski, E., Emrick, T., et al., 2010. Adsorption energy of nano- and microparticles at liquid-liquid interfaces. Langmuir 26 (15), 12518–12522. https://doi.org/10.1021/la100497h.

Fujiki, K., Tsubokawa, N., Sone, Y., 1990. Radical grafting from carbon black. Graft polymerization of vinyl monomers initiated by azo groups introduced onto carbon black surface. Polym. J. 22 (8), 661–670.

Gbadamosi, A.O., Junin, R., Manan, M.A., et al., 2018. Recent advances and prospects in polymeric nanofluids application for enhanced oil recovery. J. Ind. Eng. Chem. 66 (25), 1–19. https://doi.org/10.1016/j.jiec.2018.05.020.

Gomari, S.R., Omar, Y.G.D., Amrouche, F., et al., 2019. New insights into application of nanoparticles for water-based enhanced oil recovery in carbonate reservoirs. Colloids Surf., A 568 (5), 164–172. https://doi.org/10.1016/j.colsurfa.2019.01.037.

Han, Y., Hwang, G., Park, S., et al., 2017. Stability of carboxyl-functionalized carbon black nanoparticles: the role of solution chemistry and humic acid. Environ. Sci-Nano. 4 (4), 800–810. https://doi.org/10.1039/C6EN00530F.

Holditch, S.A., 2013. Unconventional oil and gas resource development–Let's do it right. J. Unconv. Oil. Gas. Resour. 1–2, 2–8. https://doi.org/10.1016/j.juogr.2013.05.001.

Hussain, C.M., 2018. Handbook of Nanomaterials for Industrial Applications. Elsevier. https://doi.org/10.1016/C2016-0-04427-3.

Huang, H., Guo, Z., Yang, P., et al., 2021. Electrical conductivity, oil absorption and electric heating of carbon black-modified carbon nanofibers. Chem. Res. Chin. Univ. 37 (3), 541–548. https://doi.org/10.1007/s40242-021-1109-3.

Hwang, G., Gomez-Flores, A., Bradford, S.A., et al., 2018. Analysis of stability behavior of carbon black nanoparticles in ecotoxicological media: hydrophobic and steric effects. Colloids Surf., A 554, 306–316. https://doi.org/10.1016/j.colsurfa.2018.06.049.

Jiao, F., 2019. Re-recognition of "unconventional" in unconventional oil and gas. Petrol. Explor. Dev. 46 (5), 847–855. https://doi.org/10.1016/S1876-3804(19)60244-2.

Kamkar, M., Bazazi, P., Kannan, A., et al., 2020. Polymeric-nanofluids stabilized emulsions: interfacial versus bulk rheology. J. Colloid Interface Sci. 576 (15), 252–263. https://doi.org/10.1016/j.jcis.2020.04.105.

Khaleduzzaman, S.S., Mahbubul, I.M., Shahrul, I.M., et al., 2013. Effect of particle concentration, temperature and surfactant on surface tension of nanofluids. Int. Commun. Heat. Mass. 49, 110–114. https://doi.org/10.1016/j.icheatmasstransfer.2013.10.010.

Long, C.M., Nascarella, M.A., Valberg, P.A., 2013. Carbon black vs. black carbon and other airborne materials containing elemental carbon: physical and chemical distinctions. Environ. Pollut. 181, 271–286. https://doi.org/10.1016/j.envpol.2013.06.009.

Luo, D., Wang, F., Zhu, J., 2016. Nanofluid of graphene-based amphiphilic Janus nanosheets for tertiary or enhanced oil recovery: high performance at low concentration. P. Natl. Acad. Sci. 113 (28), 7711–7716. https://doi.org/10.1073/pnas.1608135113.

Luo, D., Wang, F., Tang, L., et al., 2017. Secondary oil recovery using graphene-based amphiphilic Janus nanosheet fluid at an ultralow concentration. Ind. Eng. Chem. Res. 56 (39), 11125–11132. https://doi.org/10.1021/acs.iecr.7b02384.

Mariyate, J., Bera, A., 2021. Recent progresses of microemulsions-based nanofluids as a potential tool for enhanced oil recovery. Fuel 306 (15), 121640. https://doi.org/10.1016/j.fuel.2021.121640.

Mariyate, J., Bera, A., 2022. A critical review on selection of microemulsions or nanoemulsions for enhanced oil recovery. J. Mol. Liq. 353, 118791. https://doi.org/10.1016/j.molliq.2022.118791.

Maurya, N.K., Mandal, A., 2018. Investigation of synergistic effect of nanoparticle and surfactant in macro emulsion based EOR application in oil reservoirs. Chem. Eng. Res. Des. 132, 370–384. https://doi.org/10.1016/j.cherd.2018.01.049.

Maurya, N.K., Kushwaha, P., Mandal, A., 2017. Studies on interfacial and rheological properties of water soluble polymer grafted nanoparticle for application in enhanced oil recovery. J. Taiwan Inst. Chem. Eng. 70, 319–330. https://doi.org/10.1016/j.jtice.2016.10.021.

Mayol, J.C., Moridis, N., McVay, D.A., et al., 2020. Assessment of oil and gas resources in the vaca muerta shale, neuquén basin, Argentina. In: SPE Latin American and

Caribbean Petroleum Engineering Conference, doi:10.2118/199035-MS.
Moon, R.J., Martini, A., Nairn, J., et al., 2011. Cellulose nanomaterials review: structure, properties and nanocomposites. Chem. Soc. Rev. 40 (7), 3941–3994. https://doi.org/10.1039/C0CS00108B.
Negin, C., Ali, S., Xie, Q., 2016. Application of nanotechnology for enhancing oil recovery–A review. Petroleum 2 (4), 324–333. https://doi.org/10.1016/j.petlm.2016.10.002.
Nguele, R., Sreu, T., Inoue, H., et al., 2019. Enhancing oil production using silica-based nanofluids: preparation, stability, and displacement mechanisms. Ind. Eng. Chem. Res. 58 (32), 15045–15060. https://doi.org/10.1021/acs.iecr.9b01629.
Papirer, E., Dentzer, J., Li, S., et al., 1991. Surface groups on nitric acid oxidized carbon black samples determined by chemical and thermodesorption analyses. Carbon 29 (1), 69–72. https://doi.org/10.1016/0008-6223(91)90096-2.
Probst, N., Grivei, E., 2002. Structure and electrical properties of carbon black. Carbon 40 (2), 201–205. https://doi.org/10.1016/S0008-6223(01)00174-9.
Qiu, Z., Li, X., Wang, Y., et al., 2021. Structure and properties of polyester/carbon black system prepared by in-situ continuous polymerization. Textil. Res. J. 42 (10), 15–21. https://doi.org/10.13475/j.fzxb.20210701107.
Radnia, H., Rashidi, A., Nazar, A.R.S., et al., 2018. A novel nanofluid based on sulfonated graphene for enhanced oil recovery. J. Mol. Liq. 271, 795–806. https://doi.org/10.1016/j.molliq.2018.09.070.
Raju, A.T., Das, M., Dash, B., et al., 2022. Variation of air permeability in bromobutyl rubber/epoxidized natural rubber composites: influence of structure of filler particle. Polym. Eng. Sci. 62 (3), 718–729. https://doi.org/10.1002/pen.25879.
Rezk, M.Y., Allam, N.K., 2019. Impact of nanotechnology on enhanced oil recovery: a mini-review. Ind. Eng. Chem. Res. 58 (36), 16287–16295. https://doi.org/10.1016/J.MOLLIQ.2020.113876.
Rezvani, H., Kazemzadeh, Y., Sharifi, M., et al., 2019. A new insight into Fe_3O_4-based nanocomposites for adsorption of asphaltene at the oil/water interface: an experimental interfacial study. J. Petrol. Sci. Eng. 177, 786–797. https://doi.org/10.1016/j.petrol.2019.02.077.
Rezvani, H., Panahpoori, D., Riazi, M., et al., 2020. A novel foam formulation by Al_2O_3/SiO_2 nanoparticles for EOR applications: a mechanistic study. J. Mol. Liq. 304, 112730. https://doi.org/10.1016/j.molliq.2020.112730.
Saini, A., Tripathy, S.S., Maheshwari, P.H., et al., 2019. Surface modified exfoliated graphite as a novel adsorbent for de-fluoridation of drinking water. Mater. Res. Express 6 (8), 085605. https://doi.org/10.1088/2053-1591/ab19f7.
Salameh, M.G., 2003. Can renewable and unconventional energy sources bridge the global energy gap in the 21st century? Appl. Energy 75 (1–2), 33–42. https://doi.org/10.1016/S0306-2619(03)00016-3.
Sharma, T., Iglauer, S., Sangwai, J.S., 2016. Silica Nanofluids in an oilfield polymer polyacrylamide: interfacial properties, wettability alteration, and applications for chemical enhanced oil recovery. Ind. Eng. Chem. Res. 55 (48), 12387–12397. https://doi.org/10.1021/acs.iecr.6b03299.
Soares, M.C.F., Viana, M.M., Schaefer, Z.L., et al., 2014. Surface modification of carbon black nanoparticles by dodecylamine: thermal stability and phase transfer in brine medium. Carbon 72, 287–295. https://doi.org/10.1016/j.carbon.2014.02.008.
Sun, X., Zhang, Y., Chen, G., et al., 2017. Application of nanoparticles in enhanced oil recovery: a critical review of recent progress. Energies 10 (345), 1–33. https://doi.org/10.3390/en10030345.
Toupin, M., Bélanger, D., 2007. Thermal stability study of aryl modified carbon black by in situ generated diazonium salt. J. Phys. Chem. C 111 (14), 5394–5401. https://doi.org/10.1021/jp066868e.
Tsubokawa, N., Kuroda, A., Sone, Y., 1989. Grafting onto carbon black by the reaction of reactive carbon black having epoxide groups with several polymers. J. Polym. Sci. 27 (5), 1701–1712. https://doi.org/10.1002/pola.1989.080270521.
Wang, H., Ma, X., Tong, X., et al., 2016. Assessment of global unconventional oil and gas resources. Petrol. Explor. Dev. 43 (6), 925–940. https://doi.org/10.1016/S1876-3804(16)30111-2.
Worthen, A.J., Tran, V., Cornell, K.A., et al., 2016. Steric stabilization of nanoparticles with grafted low molecular weight ligands in highly concentrated brines including divalent ions. Soft Matter 12 (7), 2025–2039. https://doi.org/10.1039/C5SM02787J.
Xue, Z., Worthen, A., Qajar, A., et al., 2016. Viscosity and stability of ultra-high internal phase CO_2-in-water foams stabilized with surfactants and nanoparticles with or without polyelectrolytes. J. Colloid Interface Sci. 461, 383–395. https://doi.org/10.1016/j.jcis.2015.08.031.
Yao, J., Yang, M., Duan, Y.X., 2014. Chemistry, biology, and medicine of fluorescent nanomaterials and related systems: new insights into biosensing, bioimaging, genomics, diagnostics, and therapy. Chem. Rev. 114 (12), 6130–6178. https://doi.org/10.1021/cr200359p.
Zhao, G., Dai, C.L., You, Q., 2018b. Characteristics and displacement mechanisms of the dispersed particle gel soft heterogeneous compound flooding system. Petrol. Explor. Dev. 45 (3), 481–490. https://doi.org/10.1016/S1876-3804(18)30053-3.
Zhao, G., Li, J., Dai, C., et al., 2018a. Dispersed particle gel-strengthened polymer/surfactant as a novel combination flooding system for enhanced oil recovery. Energy Fuel. 32 (11), 11317–11327. https://doi.org/10.1021/ACS.ENERGYFUELS.8B02720.